Journal of Fluorescence, Vol. 5, No. 3, 1995

Spectral Inhomogeneity and Wavelength-Dependent Rotation of Probe Molecules in Membranes

N. A. Nemkovich[1] and A. N. Rubinov[1]

Received September 30, 1994; accepted October 26, 1994

Using subnanosecond laser spectrofluorometry, the spectral and polarization time-resolved characteristics of 1-phenylnaphthylamine (1-AN) fluorescent probe in phospholipid bilayer and red blood cell (RBC) membranes have been studied. It is shown that the electronic spectra of the probe in model-membranes are inhomogeneously broadened. In contrast to low-molecular weight solvents, there are two reasons for inhomogeneous broadening. The first is connected with different levels of location of probe molecules in the membrane. Inhomogeneous broadening due to the first factor has a static character. The second reason is similar to that of solutions and linked with fluctuations of solvate structure. This type of broadening has a dynamic character. The process of intermolecular relaxation in membranes is accompanied by the release of the free energy excess, which results in wavelength-dependent rotation of probe.

KEY WORDS: Fluorescent probe; spectrofluorometry; inhomogeneous broadening; fluorescence kinetics.

INTRODUCTION

In analyzing the spectral properties of a fluorescent probe in liquid media one must consider the interaction of the probe molecule with nearby molecules or their segments. In other words, instead of the fluorophore molecule itself, the whole solvate (probe molecule plus the closest molecules of surrounding medium) must be considered if one wishes to understand the spectral characteristics of a solution. Another important point is the temperature fluctuations of the microstructure of the solvates. Due to these fluctuations different solvates built up around identical probe molecules may have a different spatial structure, i.e., possess a different free energy. This factor causes the inhomogeneous broadening of electronic spectra of fluorophore molecules in a solution.

The analysis of the probe properties is very much complicated by the extremely complex dynamic behavior of liquid systems: both probes and surrounding molecules undergo a variety of processes, e.g., translation, orientation, libration, rotation of individual molecules or some of their groups. Each of these processes is characterized by its own time scale.

If the time of rearrangement of the configuration of the molecules in the solvate τ_r is substantially longer than the lifetime of the probe excited state τ ($\tau_r >> \tau$), the solvate configuration (and consequently the position of the electronic levels) does not change during the absorption–emission cycle. In this case the optical properties of a liquid solution are similar to those of a dye-doped rigid matrix with statistical variations of the structure near the fluorescent molecules. One may say that in such cases fluctuational broadening has a static character. This type of inhomogeneous broadening was discovered experimentally in Refs. 1 and 2 and manifested itself in a red shift of the stationary fluorescence spectrum of rigid dye solutions under the shift of excitation frequency to the long-wave slope of the absorption spectrum (phenomenon of so-called bathochromic luminescence).

In liquid media ($\tau_r < \tau$) the inhomogeneous broad-

[1] B. I. Stepanov Institute of Physics, Academy of Sciences of Belarus, Minsk 220072, Belarus.

1053-0509/95/0900-0285$07.50/0

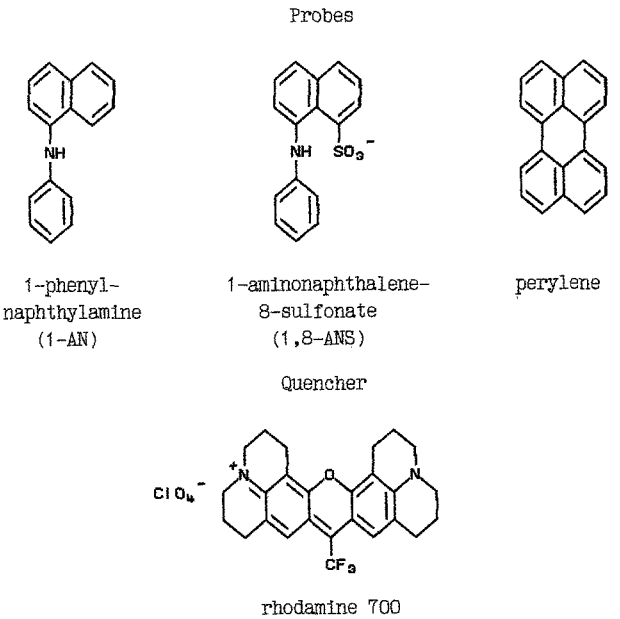

Fig. 1. Fluorescent probes and the quencher used in this work.

ening has a dynamic character. This means that the degree of observed inhomogeneity depends on the time resolution of spectroscopic measurements and on the time interval passed after the moment of excitation. The term "spectral diffusion" is also applied to describe the phenomenon of dynamic inhomogeneous spectral broadening.

A number of techniques have been used to measure dynamic inhomogeneous broadening. In 1980 Nemkovich *et al.*,[3] using a nanosecond laser spectrofluorimeter, observed for the first time that the positions of instantaneous fluorescence spectra of solution immediately after excitation depend on the exciting light frequency. Other experimental methods used to probe dynamic inhomogeneous broadening include resonance Raman scattering,[4] transient hole burning,[5,6] photon echo,[7,8] electronic excited-state energy transfer,[9,10] and time-resolved stimulated Stokes shift.[11]

Directly after excitation different solvates (or unit cells of the system) appear at different nonequilibrium Franck-Condon sublevels of the configurational continuum. If the excitation frequency is located near the absorption band maximum, the process is accompanied by the lowering of the emitted photon frequency in the course of relaxation. Other words, the shift of the fluorescence spectrum to the red is observed in this case during the time period of emission (so-called time-dependent fluorescence Stokes shift, TDFSS). Brand *et al.*[12] were the first to apply time-resolved spectroscopy and showed the nanosecond kinetics of fluorescence probe spectra in egg lecithin vesicles. The results were consistent with a kinetic model for intermolecular relaxation. Later in Ref. 13 the nanosecond shift of fluorescence probe spectra was observed by phase fluorometry. Demchenko and Shcherbatska[14] used time-resolved methods and red-edge excitation fluorescence effects for analysis of the nature and characteristic times of amphiphilic molecule motion in the polar region of a phospholipid bilayer.

In our previous papers[15–18] we studied the TDFSS and probe rotation and localization in a phospholipid bilayer and in red blood cell membranes using different excitation wavelengths. The present paper focuses on our results concerning the inhomogeneous broadening of a fluorescent probe in membranes and its rotational dynamics.

MATERIALS AND METHODS

The probe molecules studied in this work as well as the quencher molecule used in the experiments with energy transfer are given in Fig. 1. All probes were of chromotographic purity. The experiments were carried out with vesicles obtained by the conventional method[16] from egg yolk phosphatidylcholine and dimyristoylphosphatidylcholine (DMPC). Vesicles were produced by short-term (10–15 min) sonication of lipid suspension in 50 n*M* tris-HCl buffer, pH-7.4, using a 150-W ultrasonic disintegrator. The conditions for the experiments were chosen to provide the predominant formation of bilayer monolamellar vesicles. The vesicles were separated by size with a centrifuge and additionally fractioned in Sepharose 4B. Experiments were carried out with vesicles of sizes ranging from 100 nm to 200 nm at a lipid concentration of 10 mg/ml.

In the experiments with the excitation of the probe at the maximum of absorption the lipid–probe ratio was 1000:1, while at the red-edge excitation the corresponding value was close to 500:1. As was shown by preliminary studies, higher probe concentrations led to distortion of fluorescence spectra and to decrease of fluorescence polarization due to the increase of nonradiative energy transfer efficiency.

To obtain the human red blood cell membranes we used the fresh hemoglobin-free ghosts of human erythrocytes, prepared by a method originally described by Dodge *et al.*[19] All reagents and chemicals used were of the purest grade available from commercial sources. Human blood was provided by the Research Institute of

Blood and the Research Institute of Radiation Medicine of Belarus.

To investigate the TDFSS and rotational dynamics of the probe in the phospholipid bilayer membranes, a nanosecond laser spectrofluorimeter[20] was employed. The fluorescence decay studies were performed with photon counting system PRA 700. To investigate the probe rotation in the human erythrocyte ghosts an automated laser spectrofluorimeter was constructed. Its excitation part includes an atmospheric pressure nitrogen laser (pulse duration 0.35 ns, peak power 200 kW) and distributed-feedback dye laser (tuning range 400–750 nm, spectral width 0.1–0.2 nm). After the polarizer (Glan prism) the exciting radiation is focused on the sample, which is placed in front of the analyzer (another Glan prism). The recording part of the apparatus includes a double diffraction monochromator (1200 lines/mm replica, 0.6 nm/mm dispersion), fast photomultiplier (2 ns temporal resolution), and boxcar integrator (1.0 GHz transmission band). The registered signal is normalized by the signal from the photodiode, which received the fluorescence from a rhodamine 6G reference cell excited by a nitrogen laser. The full control of all optical and electronic systems of the laser spectrofluorimeter as well as the data processing were performed by an IBM PC/AT-286 computer.

The coefficients for correction of the spectral sensitivity of the detection system were determined by the conventional method, using a standard band lamp.

SPECTRAL INHOMOGENEITY OF PROBE MOLECULES

In recent years red-edge excitation spectroscopy (REES) has become widely accepted as a general spectroscopic method of investigation of solutions and other systems with inhomogeneously broadened electronic spectra.[21] The effect manifests itself in the shift of the fluorescence spectrum toward longer wavelengths under the shift of the excitation frequency to the red edge of the absorption band.

The effect of red-edge excitation on the time-resolved fluorescence spectra in comparison with steady-state spectra is less known. In the framework of the stochastic model the instantaneous fluorescence spectrum $I(\nu, t)$ is determined by convolution of an inhomogeneous broadening function (IBF) and a homogeneous spectrum:

$$I(\nu, t) = \int \rho(\nu', t) S_e(\nu - \nu')\, d\nu' \qquad (1)$$

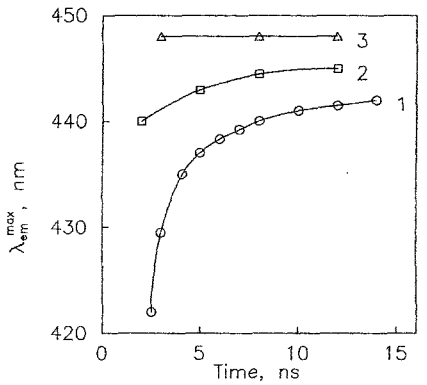

Fig. 2. The dependence of the maximum of time-resolved fluorescence spectrum on the detection time for 1-AN in glycerol at different excitation wavelengths. Curves 1–3 at λ_{ex} = 337, 400, and 416 nm, respectively.

where $\rho(\nu', t)$ is a time-dependent IBF and $S_e(\nu - \nu')$ is a homogeneous fluorescence spectrum.

At the moment of excitation ($t = 0$) the number of elementary cells in the excited state with a certain value of 0–0 transition frequency is proportional to the number of solvates in the ground state with the same 0–0 frequency and to the absorption coefficient of this type of solvate. Consequently the IBF for excited molecules at time $t = 0$ is equal to

$$\rho(\nu, 0) = \rho(\nu)\, S_a(\nu - \nu_{ex}) \qquad (2)$$

where $\rho(\nu)$ is the equilibrium IBF in the ground state, $S_a(\nu - \nu_{ex})$ is the homogeneous absorption spectrum, and ν_{ex} is the exciting light frequency. As follows from Eqs. (1) and (2), the IBF in the excited state and, correspondingly, the instantaneous fluorescence spectrum $I(\nu, 0)$ at time $t = 0$ depend on the excitation frequency.

Of course, due to the significant width of the homogeneous absorption spectrum a fairly wide distribution of solvates over configurational sublevels in the excited state is always created. However, on the red slope of the absorption spectrum there is a frequency range in which quite noticeable selectivity of excitation may be achieved.

Experimentally obtained dependences of the time-resolved fluorescence spectrum maximum on time for 1-phenylnaphthylamine (1-AN) in glycerol and in vesicles at three excitation wavelengths are shown in Figs. 2 and 3. After the excitation the magnitude of the TDFSS decreases with time for both systems, but for 1-AN in glycerol all time-resolved spectra tend to the same position independently of the excitation wavelength, while in vesicles they tend to different positions.

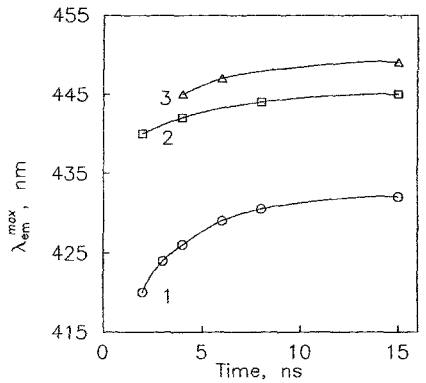

Fig. 3. The dependence of the maximum of time-resolved fluorescence spectrum on the detection time for 1-AN in phosphatidylcholine vesicles at different excitation wavelengths. Curves 1–3 at λ_{ex} = 337, 390, and 410 nm, respectively.

There is another difference in the spectral dynamics of dye fluorescence in glycerol and in vesicles. In glycerol solution the spectral kinetics of the probe completely disappears at certain excitation wavelength (416 nm), while in vesicles it is observed at all excitation wavelengths up to 410 nm, the longest wavelength which could be used in our experiments. The registration of probe fluorescence at excitation wavelengths greater than 410 nm was not possible because of the intensive light scattering in the membrane suspension.

The above effect cannot be explained by the difference of viscosity in both systems, because the microviscosity of the bilayer at room temperature, as estimated from the probe rotation, turned out to be even smaller than that of the glycerol. This disagreement in character of the TDFSS in solutions and membranes is connected with the different nature of spectral broadening in the studied systems.

As the incorporation of a probe into the membrane is a statistical process, a certain distribution of the probe over location may take place. Therefore different electrical fields may be applied to molecules at different locations. This results in statistical variation of the energy of intermolecular interactions, and, consequently, in inhomogeneous broadening of electronic spectra. In addition, at each location of the probe, fluctuations of the free energy are possible due to the segmentary dynamics of phospholipids and due to a change in the magnitude and direction of the local electric field of the membrane.

At room temperature, the time of rotational diffusion of the probe is comparable with the lifetime of its excited state, and the translational motion of the probe is much slower than the rotational one. Therefore, the inhomogeneous broadening associated with the segmentary dynamics of phospholipids and probe rotation has a dynamic character and manifests itself in the form of nanosecond TDFSS. On the other hand, the inhomogeneous broadening associated with the distribution of probe over localization depth has a static character and it is displayed as a dependence of the final position of the time-resolved fluorescence spectrum on excitation wavelength (see Fig. 3).

To prove the above explanation of probe molecule spectral inhomogeneity in vesicles we have performed special experiments based on the fluorescence energy transfer from the probe in bilayer (donor) to the quencher in buffer (acceptor).

FLUORESCENCE DECAY STUDIES OF PROBE MOLECULE LOCALIZATION

Forster resonance energy transfer has often been used to study the structure of membranes, lipoproteins, and lipid–protein complexes. A number of numerical and analytical approaches to energy transfer in two-dimensional structures have been published [22–25]. Fluorescence energy transfer in the rapid-diffusion limit is well known in biophysics. If the diffusional motions substantially change the average distance between donor and accepter during the excited-state lifetime, the energy transfer may be enhanced, but only to a certain limit. The further increase of the diffusion coefficient has no further effect on the transfer efficiency. The theoretical and experimental analysis[26] of this rapid-diffusion limit shows that the distance of the closest approach between donor and acceptor takes place in such a situation.

To measure the distance between the probe (donor) in phospholipid bilayer and water-soluble quencher (acceptor) on the membrane surface we modified the rapid-diffusion-limit approach as follows. We supposed that for realization of the "rapid-diffusion-limit" condition the diffusion of water-soluble quencher outside the phospholipid bilayer must be fast enough in comparison with characteristic time of fluorescence energy transfer. Under this condition we may consider the situation as if acceptor molecules were located directly at the surface of the bilayer. Since a water-soluble acceptor cannot penetrate inside the bilayer, the quencher molecules at the surface appear to be the closest partners for energy transfer from the probe. This means that the quencher position in the process of fluorescence energy transfer is fixed and exactly known.

Now the distance r between the position of the probe molecule and the bilayer surface may be derived

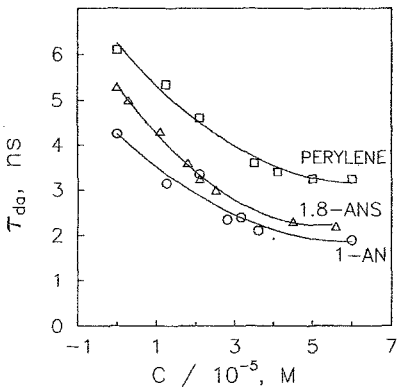

Fig. 4. Dependence of the fluorescence lifetime of the probe molecules in vesicles versus concentration of quencher in buffer.

Table I. Depth of the Probe Location in Egg Phosphatidylcholine Vesicles (r), Forster Radius (R_0), and Donor Quantum Yield (F_d) in the Absence of Energy Transfer[a]

Donor–acceptor pair	r (nm)	R_0 (nm)	F_d
1–AN–Rh700	2.10	1.80	0.22
1,8–ANS–Rh700	0.70	2.10	0.30
Perylene–Rh700	2.35	2.75	0.95

[a] Excitation at 337 nm, T = 22°C, refractive index n = 1.33 [26].

Table II. Depth of the 1-AN Location in Dimyristoylphosphatidylcholine vesicles (r), Forster Radius (R_0), and Dielectric Constant (ε) Estimated for Different Excitation Frequency (ν_{ex})[a]

ν_{ex} (10^3 cm^{-1})	ν_{fl} (10^3 cm^{-1})	r (nm)	R_0 (nm)	ε
30.3	24.0	2.3	1.8	9.1
29.4	23.8	2.1	1.8	10.4
28.6	23.8	2.1	1.8	10.4
27.8	23.8	2.1	1.8	10.4
26.7	23.7	1.9	1.9	11.4
26.3	23.5	1.7	2.1	14.3
25.6	23.1	0.57	2.4	24.5

[a] ν_{fl} is the fluorescence spectrum maximum; T = 22°C.

as follows. First, the fluorescence lifetime τ_{da} of the donor in the case of energy transfer influence is assumed to follow the well-known equation

$$\tau^{-1}_{da} = \tau^{-1}_{d} + \tau^{-1}_{d} (R_0/r)^6 \quad (3)$$

where τ_d is the donor excited-state lifetime in the absence of energy transfer and R_0 is the Forster radius, i.e., the distance at which the transfer rate equals the donor decay rate. Second, the experimentally measured fluorescence decay curve of the donor may be approximated by the two-exponential law

$$I_m(t) = A_1 \cdot \exp(-t/\tau_1) + A_2 \cdot \exp(-t/\tau_2) \quad (4)$$

where $A_{1,2}$ and $\tau_{1,2}$ are the experimental parameters of the donor fluorescence decay. The values of r were obtained from Eq. (3). For such a purpose the donor fluorescence lifetimes τ_{da} and τ_d were calculated from the formula

$$\tau_{da,d} = \int_0^\infty t I_m(t)\, dt \Big/ \int_0^\infty I_m(t)\, dt \quad (5)$$

As a water-soluble quencher we used rhodamine 700 (see Fig. 1). The Forster radius for all donor–accepter pairs was chosen to be less than half of the bilayer thickness to avoid the possible energy transfer from the opposite side of the bilayer. Figure 4 shows the results for 1-AN, 1-anilinonaphthalene-8-sulfonate (1,8-ANS), and perylene fluorescence quenching by rhodamine 700 of different concentrations in buffer. It is seen from the figure that at concentrations of rhodamine 700 greater than 5×10^{-5} M the saturation effect takes place, i.e., τ_{da} is practically independent of the concentration of quencher. This is the indication that the above "rapid-diffusion-limit" condition of energy transfer is satisfied.

The results on the probe and quencher separation measurements are presented in Table I. It is interesting to note that all estimated values of r are in agreement with physicochemical expectations. For example, perylene is a nonpolar probe and it must be located in the middle part of the bilayer. As follows from Table I, for perylene r = 2.35 nm, and this value is roughly equal to half of the bilayer thickness. On the other hand, 1,8-ANS is a charged probe and it must be located closer to the polar heads of phospholipids than the electrically neutral dipole probe 1-AN. Such a conclusion is also in agreement with the data presented in Table I.

The distribution of 1-phenylnaphthylamine molecules along bilayer was studied in dimyristoylphosphatidylcholine bilayer vesicles. Table II gives the calculated values of the probe depth localization r versus excitation frequency. As follows from Table II, the depth of probe localization at the Stokes excitation is 2.1 nm. The shift of the excitation frequency to the red slope of the probe absorption spectrum (ν_{ex} = 25,600 cm^{-1}) leads to a significant decrease of the probe localization depth down to 0.57 nm. This effect is connected with a static inhomogeneous broadening of the probe spectra and is caused by the selective excitation of "red" elementary sites located near the polar heads of phospholipid molecules.

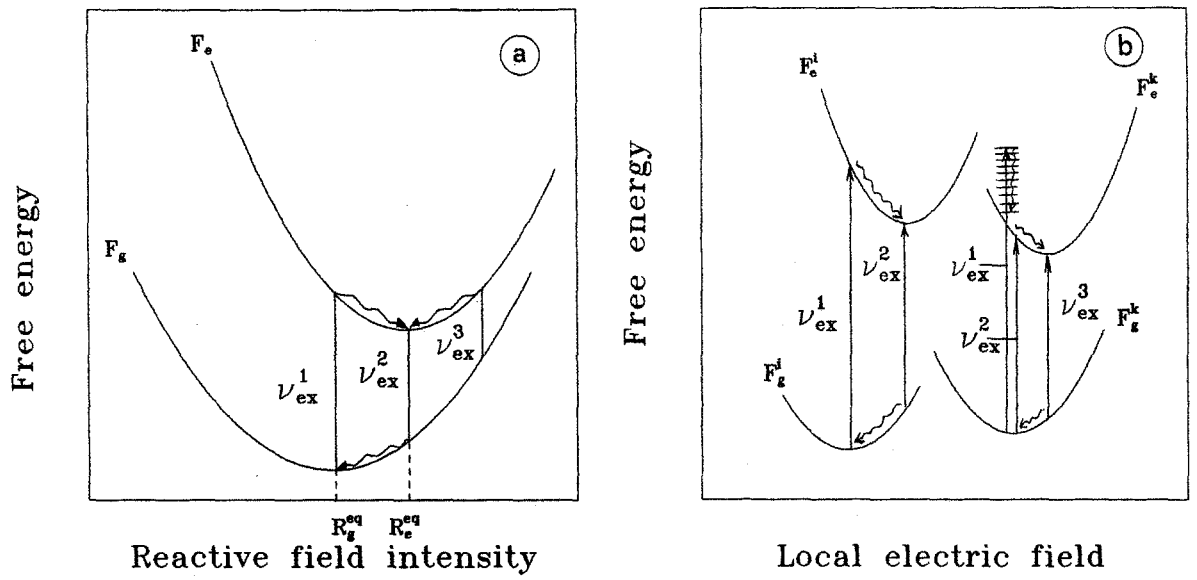

Fig. 5. The free-energy diagram of a fluorescent probe. (a) Probe in polar solvent. (b) Probe in vesicles. At the excitation frequency ν_{ex}^1 the vibrational sublevels are shown on the right pair of curves (see explanation in text).

The lack of knowledge about the local dielectric constant of lipid bilayer has so far limited progress in developing understanding about interactions among membrane proteins. In the last column of Table II the values of the dielectric constant ε of vesicles are presented as calculated by the Bakhshiev–Lippert equation:

$$\nu_a - \nu_f = [2\ (\mu_e - \mu_g)^2/hc\alpha^3]\ [(\varepsilon-1) - (n^2 - 1)/(2n^2 + 1)] \quad (6)$$

where ν_a and ν_f are the wavenumbers of the absorption and luminescence spectrum maxima, μ_e and μ_g are the electric dipole moments of the probe in excited and ground states, n is the refractive index, α is the probe cavity radius, h is the Planck constant, and c is the light velocity. It is seen that ε rapidly increases with decreasing probe depth localization.

The results obtained in this section prove that there exists a 1-AN molecule distribution along the polar region of the phospholipid bilayer. This distribution causes static inhomogeneous broadening of the electronic spectra.

FREE-ENERGY DIAGRAM FOR PROBE IN MEMBRANE

In our previous work[16,21,27] we proposed a free-energy diagram for the description of effects of spectroscopic inhomogeneous broadening in polar solutions. The diagram (see Fig. 5a) describes the dependence of the solvate free energy on the local reactive field strength. The reactive field R in the solvates serves here as a generalized coordinate which describes the effect of the local microstructure of the solvent on the fluorescent molecule. For simplicity, the vibrational broadening of the electronic levels is not shown here.

Each point on the curves describing $F_g(R)$ and $F_e(R)$ corresponds to a particular type of solvate with the field R. Since the reactive field of the solvate has no time to change during the electronic transition (except for its electronic component, which can be ignored for polar solutions), electronic transitions are represented in the diagram by vertical arrows (intermolecular interpretation of the Frank–Condon principle).

As follows from the diagram (Fig. 5a), a decrease of the excitation frequency in rigid solvents (where emission occurs from the same configurational state of the solvate to which it was excited initially) should lead to a red shift of the steady-state fluorescence spectrum. Analysis of the diagram shows also that when the excitation frequency corresponds to ν_{ex}^1 the process of solvate relaxation is expected to be followed by a red shift of the instantaneous fluorescence spectrum. There is a particular frequency ν_{ex}^2 on the diagram, on excitation at which the solvate immediately finds itself in the equilibrium state and therefore the spectrum relaxation does not occur.

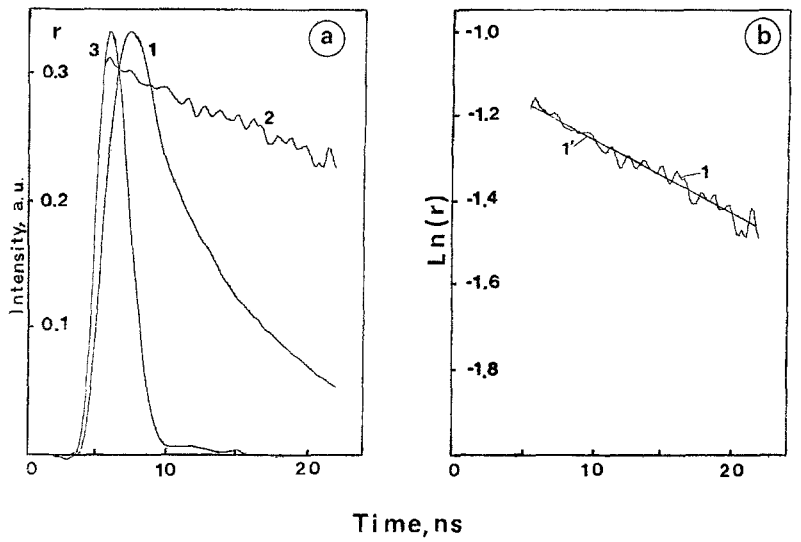

Fig. 6. Kinetics of emission anisotropy of 1-AN in glycerol at room temperature (excitation wavelength 337.1 nm), (a) The kinetics of fluorescence (1), emission anisotropy (2), and the excitation pulse (3). (b) Kinetics of emission anisotropy on a semilogarithmic scale (1) and its approximation (1') by the least-squares method.

The free-energy diagram for the probe–environment centers (solvates) in vesicles, plotted for simplicity only for two different depths of probe location, is shown in Fig. 5b. Here the local electric field serves as a generalized coordinate characterizing the configurational states of the solvates. This parameter varies due to fluctuation of the probe location depth and lipid segmental motion. The free energy in each electronic state is represented by a curve with a minimum corresponding to a most stable probe–environment configuration in which all the electric forces determining the intermolecular interaction are compensated.

As mentioned above, the probe instantaneous spectra in vesicles after excitation at the maximum and at the red slope of absorption spectrum relax to different positions (Fig. 3). To explain such a phenomenon, it should be assumed that the inhomogeneous broadening function caused by the statistical distribution of the probe along a bilayer in a membrane is wider than the IBF caused by the fluctuations of the solvate structure within the same depth of probe location. At such a condition, independent of the light frequency we excite the mixture of probe molecules corresponding to different locations and different configurational states of solvates. It is clear that at higher frequency (arrows ν_{ex}^1 in Fig. 5b) the solvates situated at different ("blue" and "red") depths of location appear to be mostly in nonequilibrium configurational states. In this case the range of the spectral shift during the relaxation process is expected to be largest.

Let us consider another case, when the excitation frequency is smaller (arrows ν_{ex}^2 in Fig. 5b). In this case we obtain in the excited state a mixture of equilibrium "blue" (left pair of curves on Fig. 5b) and nonequilibrium "red" (right pair of curves on Fig. 5b) solvates. Evidently the range of the temporal shift in such a case will be comparatively smaller and the time-resolved spectra relax to another position (Fig. 3).

WAVELENGTH-DEPENDENT ROTATION OF PROBE MOLECULES

Excitation at the absorption band maximum by the frequency ν_{ex}^1 (see Fig. 5) is immediately followed by configurational relaxation during which a free-energy excess is realized in the solvate. This may produce local "heating" of the solvate which is able to accelerate the probe rotation, producing additional fluorescence depolarization. During relaxation the time-resolved spectrum is shifted to longer wavelengths and the magnitude of the additional depolarization must therefore be greater at the long-wave part of the fluorescence spectrum.

The kinetics of emission anisotropy of 1-phenylnaphthylamine in glycerol (see Fig. 6), measured at excitation near the absorption maximum, within experimental error is monoexponential with a Brownian rotation time 63 ± 4 ns. The emission anisotropy at the initial moment is close to the limiting value $r_0 = 0.3$.

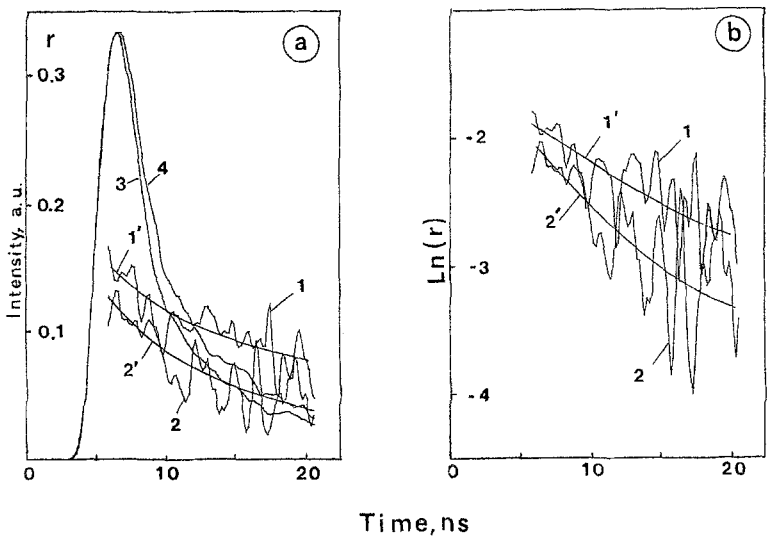

Fig. 7. (a) Kinetics of emission anisotropy of 1-AN in vesicles (22°C, λ_{ex} = 337 nm) registered on the blue (430 nm, curve 1) and the red (485 nm, curve 2) slopes of the fluorescence spectrum and its approximation by the least-square method (curves 1' and 2'). Curves 3 and 4 are the kinetics of fluorescence decay at 430 and 485 nm, respectively. (b) Kinetics of emission anisotropy on a semilogarithmic scale registered at 430 nm (1) and 485 nm (2) and its approximation (1', 2') by the least-squares method.

On the other hand, the decay of the emission anisotropy of probe in lecithin vesicles is nonexponential and depends on the excitation and detection wavelengths (see Fig. 7). As seen from Fig. 7, the anisotropy kinetics reveals a fast subnanosecond part. We were unable to record this subnanosecond component due to limiting time resolution of our setup. But the presence of this fast component of fluorescence depolarization is indicated by the observed difference between the limiting value r_0 = 0.3 of anisotropy and the measured value $r \cong 0.15$ at initial moment in the vesicles (Fig. 7). This effect is more pronounced at the red slope of the fluorescence spectrum (Fig. 7, curve 2) than at the blue one (curve 1). The experiments show that the subnanosecond component is more pronounced at excitation at λ_{ex} = 395 nm (Fig. 8) and slows down on cooling of the membrane suspension or at the red-edge excitation of the probe in vesicles in the region of the 0–0 transition.

The data confirm that there exists, in addition to Brownian diffusion, rotation of the probe in vesicles. The magnitude of this rotation during the relaxation period depends on the amount of realized free energy. Such an effect can be regarded as wavelength-dependent rotation and it was observed earlier[27,28] in a polar solutions of phthalimides. More likely the phenomenon of wavelength-dependent rotation is a universal one and should be taken into account when considering the spectroscopic properties of different liquid systems which include dye molecules with inhomogeneously broadened spectra.

The peculiarity of wavelength-dependent rotation of the probe in a membrane is connected with its (membrane) specific structure, in particular, with rigid the arrangement of phospholipid molecules in a bilayer. It seems that the probe itself is more mobile than the surrounding lipid segments. The absence of wavelength-dependent rotation of 1-phenylnaphthylamine in glycerol is likely to be associated with the realization in the solution of the stick boundary condition.[16]

To check the universal character of wavelength-dependent rotation of probe molecules we studied the kinetics of emission anisotropy and instantaneous emission anisotropy spectra for 1-AN in ghosts of human erythrocytes.

The isolation of the erythrocyte membrane is fundamental to the detailed study of its structure and dynamics. The term "ghost" is used in preference to "membranes" for the description of the delicate discoid bodies obtained after the removal of the hemoglobin from the erythrocytes.

The results we have obtained on the time-resolved fluorometry of human erythrocyte ghosts show that the instantaneous fluorescence spectra of a probe experience a shift on a nanosecond time scale, as in vesicles. The fluorescence decay is nonexponential and the emission lifetime depends on the detection wavelength. Such effects are evidence of intermolecular configurational re-

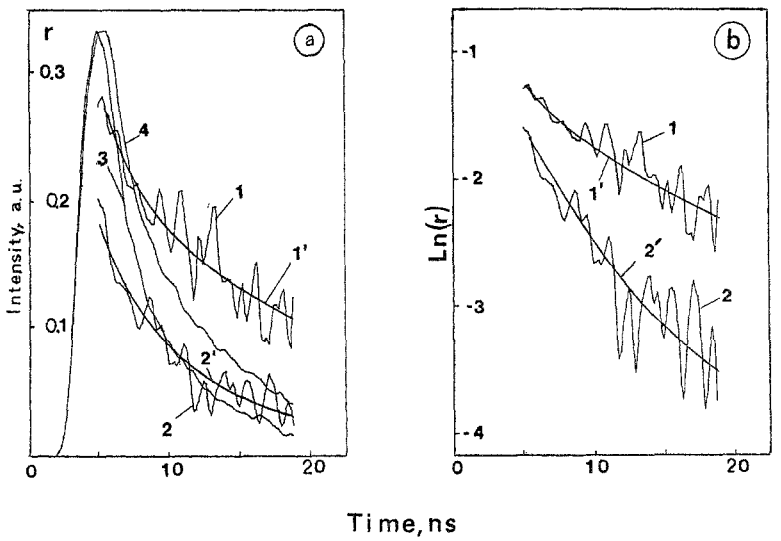

Fig. 8. Kinetics of fluorescence and anisotropy of 1-AN in vesicles at 22°C (excitation wavelength 395 nm). (a) The kinetics of fluorescence (curves 3 and 4) and emission anisotropy registered on the blue (430 nm, curve 1) and the red (475 nm, curve 2) slopes of the fluorescence spectrum and its approximation (1', 2') by the least-squares method. (b) Kinetics of emission anisotropy in a semilogarithmic scale registered at the wavelength 430 nm (curve 1) and 475 nm (curve 2) and its approximation (1', 2') by the least-squares method.

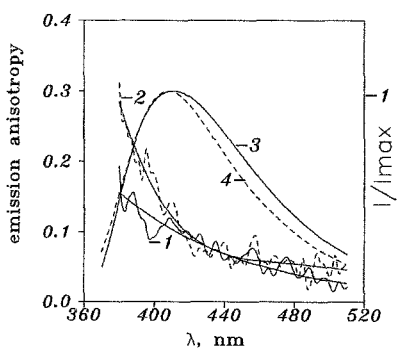

Fig. 9. Instantaneous anisotropy spectra (curves 1 and 2) and steady-state fluorescence spectra (curves 3 and 4) of 1-phenylnaphthylamine in hemoglobin-free ghosts of human erythrocytes. The difference between curves 1 and 2 demonstrates the divergence between a healthy individual and a patient exposed to low-dose radiation due to clean up work following the Chernobyl accident.

laxations occurring on the nanosecond time scale simultaneously with fluorescence decay.

The most interesting results obtained for 1-AN in erythrocyte ghosts are presented in Fig. 9. As is seen from the figure, the instantaneous values of emission anisotropy at the initial moment of time (curves 1 and 2) increase with the shift to the blue region of the fluorescence spectrum. This is a decisive indication of the wavelength-dependent rotation of probe molecules.

According to our measurements the emission anisotropy of erythrocyte ghosts of the patient is close to the limiting value $r_0 = 0.3$ for 1-phenylnaphthylamine at a wavelength of 380 nm (curve 2). On the other hand, the decay of the probe emission anisotropy of a healthy individual at $\lambda = 380$ nm is much faster and the instantaneous value (curve 1) is only $r \cong 0.15$. It is interesting to note that the position and the half-width of the steady-state fluorescence spectra of the healthy individual (curve 3) and of the patient (curve 4) are also different.

CONCLUSIONS

Inhomogeneous broadening affects significantly the spectroscopic properties of the probe molecules in bilayer phospholipid membranes, such as the time-dependent fluorescence Stokes shift, the kinetics of fluorescence and emission anisotropy, etc.

The process of intermolecular relaxation in membranes is accompanied by the release of the free-energy excess, which results in wavelength-dependent rotation of the probe. This process causes the rapid subnanosecond kinetics of fluorescence anisotropy and explains its nonexponential character. As a consequence the specific dependence of fluorescence depolarization rate on the excitation and emission wavelength is observed. The effect of wavelength-dependent rotation of the probe is most pronounced when the recording is carried out at the long-wave part of the fluorescence spectrum and the

excitation frequency is located near the absorption maximum. It vanishes at the red-edge excitation.

ACKNOWLEDGMENTS

The skillful experimental work of Dr. D. M. Gakamsky, M. G. Savvidi, and A. S. Kozlovski is gratefully acknowledged. The authors thank Dr. N. V. Shcherbatska and Yu. V. Kruchenok for preparing vesicles and ghosts of human erythrocytes. This work was supported in part by a Meyer Foundation Grant awarded by the American Physical Society.

REFERENCES

1. A. N. Rubinov and V. I. Tomin (1970) *Opt. Spectrosk.* **29,** 1082–1086.
2. W. C. Galley and R. M. Purkey (1970) *Proc. Natl. Acad. Sci. USA* **67,** 1116–1121.
3. N. A. Nemkovich, V. I. Matseiko, and V. I. Tomin (1980) *Opt. Spectrosk.* **49,** 274–282.
4. A. B. Myers, M. O. Trulson, and R. A. Mathies (1985) *J. Chem. Phys.* **83,** 5000–5006.
5. C. H. Brito-Cruz, R. L. Folk, W. H. Knox, and C. V. Shank (1986), *Chem. Phys. Lett.* **132,** 341–344.
6. J. Yu and M. Berg (1992) *J. Chem. Phys.* **96,** 8741–8749.
7. P. C. Becker, H. L. Fragnito, J.-Y. Bigot, C. H. Brito-Cruz, R. L. Folk, and C. V. Shank (1989) *Phys. Rev. Lett.* **63,** 505–510.
8. R. Zhang, T.-S. Yang, and A. B. Myers (1993) *Chem. Phys. Lett.* **211,** 541–548.
9. A. D. Stein and M. D. Fayer (1991) *Chem. Phys. Lett.* **176,** 159–166.
10. A. D. Stein and M. D. Fayer (1992) *J. Chem. Phys.* **97,** 2948–2962.
11. G. J. Blanchard (1991) *J. Chem. Phys.* **95,** 6317–6325.
12. R. P. Detoma, J. Hamilton, and L. Brand (1976) *J. Am. Chem. Soc.* **98**(16), 5001–5007.
13. E. D. Matayoshi and A. M. Kleinfeld (1981) *Biochim. Biophys. Acta* **644,** 233–241.
14. A. P. Demchenko and N. V. Shcherbatska (1985) *Biophys. Chem.* **22,** 131–143.
15. N. A. Nemkovich, E. V. Guseva, A. P. Demchenko, A. N. Rubinov, and N. V. Shcherbatska (1990) *J. Prikl. Spectrosk.* **52,** 560–566.
16. D. M. Gakamsky, A. P. Demchenko, N. A. Nemkovich, A. N. Rubinov, V. I. Tomin, and N. V. Shcherbatska (1992) *Biophys. Chem.* **42,** 49–61.
17. N. A. Nemkovich (1993) *Proc. SPIE* **1922,** 209–218.
18. N. A. Nemkovich, A. N. Rubinov, and M. G. Savvidi (1992) *Inst. Phys. Conf. Ser.* **126,** 639–642.
19. J. T. Dodge, C. Mitchell, and D. J. Hanahan (1963) *Arch. Biochem. Biophys.* **100,** 385–396.
20. D. M. Gakamsky, N. A. Nemkovich, A. N. Rubinov, V. I. Tomin, and E. V. Chaikovsky (1986) *Kvantov. Elektron.* **13,** 2271–2277.
21. N. A. Nemkovich, A. N. Rubinov, and V. I. Tomin (1991) in J. R. Lakowicz (Ed.), *Topics in Fluorescence Spectroscopy, Vol. 2: Principles*, Plenum Press, New York, pp. 367–428.
22. B. K.-K. Fung and L. Stryer (1978) *Biochemistry* **17,** 5241–5248.
23. P. K. Wolber and B. S. Hudson (1979) *Biophys. J.* **28,** 197–210.
24. T. G. Dewey and G. Hammes (1980) *Biophys. J.* **32,** 1023–1034.
25. M. C. Doody, L. A. Sklar, H. J. Pownal, J. T. Sparrow, A. M. Gotto, and L. C. Smith (1983) *Biophys. Chem.* **17,** 139–152.
26. D. D. Thomas, W. F. Carlsen, and L. Stryer (1978) *Proc. Natl. Acad. Sci. USA* **75,** 5746–5750.
27. D. M. Gakamsky, N. A. Nemkovich, and A. N. Rubinov (1992) *J. Fluoresc.* **2,** 81–92.
28. D. M. Gakamsky, N. A. Nemkovich, A. N. Rubinov, and V. I. Tomin (1988) *Opt. Spectrosk.* **64,** 678–681.